RF Propagation in Finite Thickness Unidirectional Magnetic Photonic Crystals

Gokhan Mumcu, *Student Member, IEEE*, Kubilay Sertel, *Member, IEEE*, John L. Volakis, *Fellow, IEEE*, Ilya Vitebskiy, and Alexander Figotin

***Abstract*—This paper presents an analysis of a new class of magnetic photonic crystals (MPCs) constructed from periodic arrangements of available (possibly anisotropic) homogeneous material layers. Earlier, analytical studies of semi-infinite versions of these crystals demonstrated that they exhibit the phenomena of minimal reflection at their interface, large amplitude growth of the harmonic wave within the crystal, and concurrent group velocity slow-down. These characteristics are associated with the so called frozen mode and occur at a specific frequency associated with a stationary inflection point within the Bloch diagram. In this paper, we present a characterization of these phenomena for a practical, finite thickness crystal slab and propose a realizable combination of materials consisting of available ferrite and dielectric media. The existence of significant wave amplitude growth and slow down are verified for materials with realistic losses. In addition, we identify and characterize the bandwidth of the magnetic photonic crystals and examine its relationship to the amplitude growth.**

***Index Terms*—Brillouin zone, electromagnetic propagation, frozen mode, periodic structure, photonic crystal, radiation.**

I. Introduction

MATERIAL mixtures offer unique radio frequency (RF) properties. For example, material properties such as those found in ferrites [1], [2], loaded ferrites, and ferroelectrics [3] have already been exploited in phase shifters [4], antenna miniaturization, and beam control. For the latter case, several recent studies have been published [5]–[7], where ferrite substrates and superstrates were found attractive. There is also a strong interest in the modification of materials (either by introducing periodic voids or by mixing several known materials) to realize new properties as in the case of metamaterials. A specific example is a periodic structure that exhibits forbidden propagation bands (Yablonovitch [8]). Among other examples, we can mention left handed materials [9], electromagnetic bandgap structures [10], high impedance ground planes [11], and artificial substrates for antenna arrays [12].

There is no doubt that material modifications offer unique and highly sought advantages in RF applications [13]. Nevertheless, defining the suitable material mixtures to satisfy the given design criteria is an exceedingly difficult task. For RF applications, we often seek phase shifter and antenna size reduction [14], greater focusing and sensitivity, radiation control and impedance matching. Materials that can deliver these desirable properties can make a significant impact in our design capabilities. In this regard, composite metamaterials or artificial magneto-electric media (where $\mathbf{E}$, $\mathbf{D}$, $\mathbf{B}$, and $\mathbf{H}$ are all coupled) possibly containing nano-composites, magneto-dielectric textures, or photonic crystals either in periodic or aperiodic form have been shown to exhibit unconventional new properties [15], [16]. Therefore, they hold promise in designing new devices with greater functionality. Recently, Figotin *et al.* [16] demonstrated that magnetic photonic crystals (MPCs) can display one-way transparency and wave slow-down. At RF frequencies, such composites allow for the realization of electromagnetic unidirectionality (a phenomenon which permits propagation only in one of two opposite directions). An important aspect of these MPCs is that they can be constructed from readily available materials. Also, magnetic bias could allow for tuning, thus, providing greater bandwidth realizations [17]. The one way transparency and wave slow-down, coupled with large field amplitudes was already presented in [17] for a semi infinite slab (halfspace). Thus, the analysis in [17] did not allow for an understanding of the MPC in a practical setting. Toward this goal, here we consider the propagation of electromagnetic pulses through a finite MPC slab formed by a periodic arrangement of ferromagnetic and anisotropic dielectric layers.

II. Wave Propagation in Finite Layered Media

A. Characteristics of Magnetic Photonic Crystals

Electromagnetic wave propagation in multilayered anisotropic media can be efficiently analyzed using the transfer matrix formalism [18]. In this context, the field values at the layer boundaries can be calculated through successive multiplications of the specific layer transfer matrices. For example, let us consider a one-dimensional (1D) periodic medium oriented along the z direction as shown in Fig. 1. Allowable propagation bands for this structure can be determined by making use of Bloch's theorem together with the transfer matrix $(\bar{\mathbf{T}})$ of the unit cell (a periodic element of the crystal). In accordance with Bloch's theorem (an $e^{-i\omega t}$ time convention is assumed and suppressed), electromagnetic fields propagating along the z axis can be represented as a linear superposition of the Bloch eigenmodes satisfying the periodic relation

$$\begin{bmatrix}\mathbf{E}(z+L)\\ \mathbf{H}(z+L)\end{bmatrix} = \begin{bmatrix}\mathbf{E}(z)\\ \mathbf{H}(z)\end{bmatrix} e^{ikL} \tag{1}$$

where k is the propagation constant and L is the length of the unit cell. Since the transfer matrix of a unit cell relates the field

Manuscript received August 17, 2004; revised June 17, 2005. This work was supported by the U.S. Air Force Office of Scientific Research under the Grant FA9550-04-1-0359.

G. Mumcu, K. Sertel and J. L. Volakis are with the ElectroScience Laboratory, The Ohio State University, Columbus, OH 43212 USA (e-mail: mumcu.1@osu.edu).

I. Vitebskiy and A. Figotin are with the University of California at Irvine, Irvine, CA 92717 USA.

Digital Object Identifier 10.1109/TAP.2005.859764

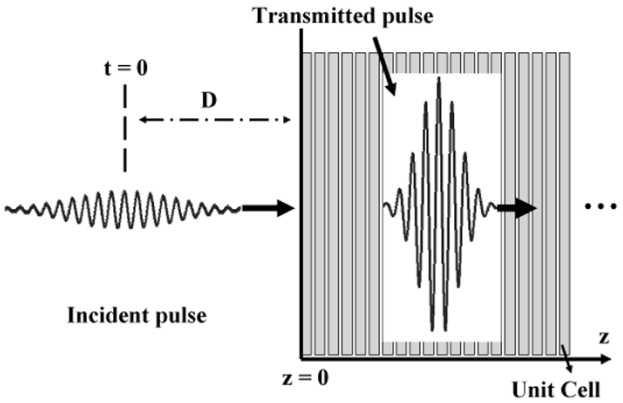

Fig. 1. Semi-infinite 1-D periodic medium.

at z to the field at $z+L$ (i.e., $\bar{\mathbf{T}}(z+L,z)$), the above equation can be recast into

$$[\bar{\mathbf{T}}(z+L,z) - \bar{\mathbf{I}}e^{ikL}]\begin{bmatrix}\mathbf{E}(z)\\ \mathbf{H}(z)\end{bmatrix} = 0 \tag{2}$$

where $\bar{\mathbf{I}}$ is the identity matrix. We readily identify from (2) that the eigenvalues of $\bar{\mathbf{T}}$ are e^{ikL} and are therefore of unity magnitude for k real corresponding to propagating waves. Non-unity eigenvalues are associated with evanescent waves and we note that (2) leads to the same fields for k and $k+2\pi n/L$ (n is an integer). Thus, it is convenient to restrict k within the range $-\pi/L \le k \le \pi/L$ without loss of information. This region is referred to as the first Brillouin zone, and can be scaled within the range of $-\pi$ to π by introducing the dimensionless wavevector $K = kL$. Every K value outside the first Brillouin zone can, of course, be plotted within the range of $-\pi$ to π by shifting it in multiples of 2π.

Throughout the paper, K will be referred to as the Bloch wavenumber, and as usual the corresponding eigenvector will define the polarization of the field for that wavenumber. Fig. 2(a) is an example of the reduced zone representation of the Bloch diagram for an anisotropic continuous medium in 0–20 GHz frequency range. This representation is typically referred to as the dispersion relation for the subject medium. In this medium, four different Bloch modes may exist, two of them propagate along $+z$ direction and the other two along $-z$. Each of the modes form a branch in the dispersion diagram and their corresponding group velocities may be found by taking the derivatives of the dispersion curve with respect to the wavenumber. For reciprocal materials (symmetric k-ω diagram), the $+z$ and $-z$ propagating modes have the same group velocities. Fig. 2(b) shows the (reduced) Brillouin zone dispersion diagram for a reciprocal *periodic* medium where two anisotropic layers form the unit cell. As seen, for this periodic crystal there are no propagating waves within a certain frequency interval, referred to as the *bandgap* region. A more interesting k-ω relation is observed for the MPC medium shown in Fig. 2(c) which is the focus of this paper. Of importance is that within the MPC, the group velocities of the $+z$ and $-z$ propagating waves are different from each other at the same frequency. Clearly, this kind of behavior implies non-reciprocal responses to incident radiation and is essential in realizing the unidirectionality property of such crystals.

In the following, we examine the propagation characteristics of a wave within a finite length MPCs made up of N unit cells as

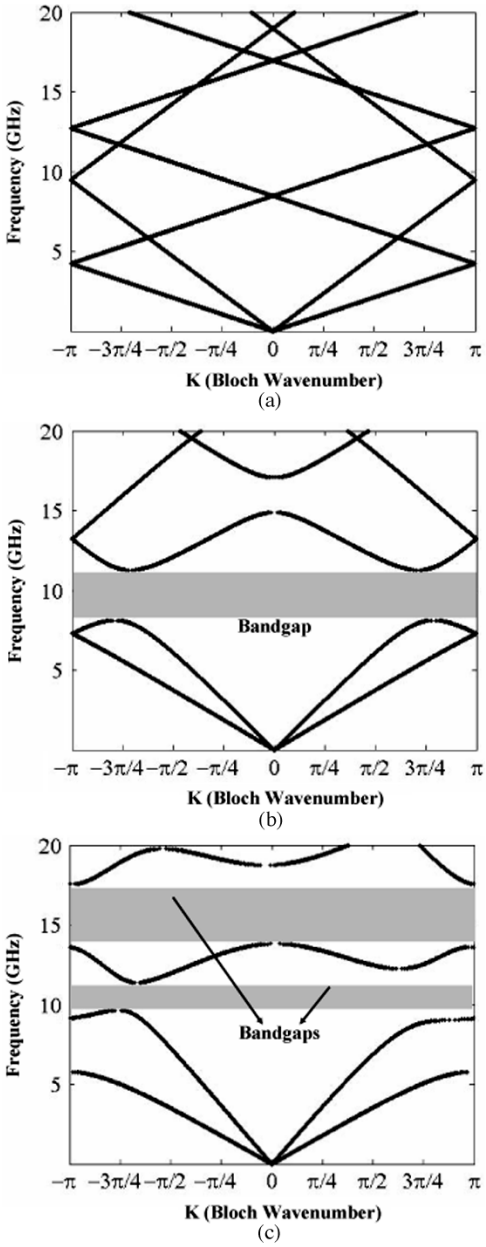

Fig. 2. Bloch dispersion relations of a periodic layered medium with primitive cells consisting of (a) a single anisotropic layer, (b) two anisotropic layers, and (c) two anisotropic and one magnetic layers.

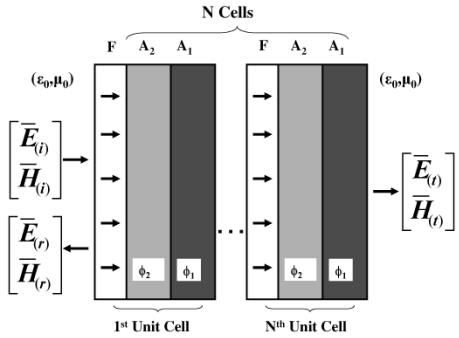

Fig. 3. Finite magnetic photonic crystal.

shown in Fig. 3 (this is the simplest possible medium exhibiting an asymmetric dispersion relation). The unit cell is composed of two identical misaligned anisotropic dielectric layers (the A

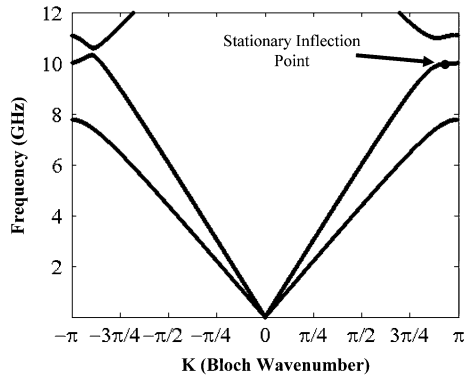

Fig. 4. Band diagram of the infinite magnetic photonic crystal, $\epsilon_a = 125$, $\delta = 40$, $\phi_{A1} = 0$, $\phi_{A2} = -\pi/12$, $L_A = 0.5695$ mm for the A layers, $\epsilon_f = 14.5$, $\mu = 1.6701$, $\beta = 0.4497$, $L_F = 0.3795 L_A$ for the F layers.

layers) and a ferromagnetic layer (the F layer). The magnetization direction of the F layers is also shown in Fig. 3. The constitutive tensors for the A layers are of the form

$$\bar{\bar{\epsilon}}_A = \epsilon_0 \begin{bmatrix} \epsilon_a + \delta\cos 2\phi_A & \delta \sin 2\phi_A & 0 \\ \delta \sin 2\phi_A & \epsilon_a - \delta \cos 2\phi_A & 0 \\ 0 & 0 & \epsilon_{az} \end{bmatrix} \tag{3a}$$

$$\bar{\bar{\mu}}_A = \mu_0 \begin{bmatrix} 1 & 0 & 0 \\ 0 & 1 & 0 \\ 0 & 0 & 1 \end{bmatrix} \tag{3b}$$

and likewise the F layers have the material properties as

$$\bar{\bar{\epsilon}}_F = \epsilon_0 \begin{bmatrix} \epsilon_f & 0 & 0 \\ 0 & \epsilon_f & 0 \\ 0 & 0 & \epsilon_{fz} \end{bmatrix} \tag{4a}$$

$$\bar{\bar{\mu}}_F = \mu_0 \begin{bmatrix} \mu & i\beta & 0 \\ -i\beta & \mu & 0 \\ 0 & 0 & \mu_{fz} \end{bmatrix}. \tag{4b}$$

We note that the F layers may also consist of gyroelectric materials, but in the microwave range our interest is only in gyromagnetic media as given above. Fig. 4 shows an example band diagram for the infinite MPC medium. In this plot, of particular interest is the inflection region. Moreover, with a proper design of the physical dimensions of the unit cell the inflection region can be tuned to have a "stationary" inflection point associated with the conditions $\omega'(k) = \omega''(k) = 0$, and $\omega'''(k) \neq 0$. This region of the band diagram is referred to as the frozen mode regime since (among other characteristics) the group velocity approaches to zero at frequencies near the stationary point. Hence, the RF pulse slows down and its amplitude grows significantly (see Fig. 1 for illustration). Below, we consider the analysis of a finite slab composed of the nonreciprocal MPC unit cell with particular emphasis on wave propagation near the frozen mode regime.

B. Analysis of 1D Magnetic Photonic Crystals

To carry out the analysis of a layered medium such as the one in Fig. 3, we start by expressing the fields as a sum of four plane wave modes: $\mathbf{v}_1 e^{iq_1 z}$, $\mathbf{v}_2 e^{-iq_1 z}$, $\mathbf{v}_3 e^{iq_2 z}$, and $\mathbf{v}_4 e^{-iq_2 z}$, where q_1 and q_2 are the supported wavenumbers and $\mathbf{v}_j$ denotes the jth electromagnetic eigenmode in free space. Specifically, we

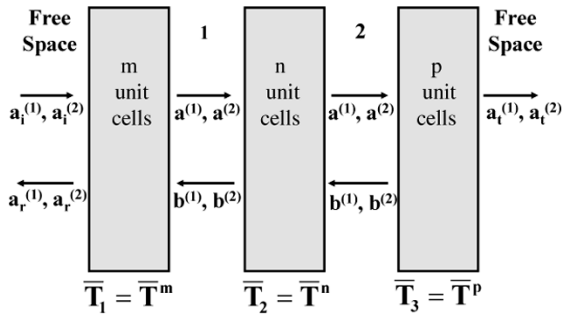

Fig. 5. Stack of multiple cells grouped to overcome matrix instabilities in slabs with many unit cells.

represent the incident, reflected, and transmitted waves at the boundaries of the MPC as

$$\begin{bmatrix} \mathbf{E}_i \\ \mathbf{H}_i \end{bmatrix} = a_i^{(1)} \mathbf{v}_1 + a_i^{(2)} \mathbf{v}_3 \tag{5a}$$

$$\begin{bmatrix} \mathbf{E}_r \\ \mathbf{H}_r \end{bmatrix} = a_r^{(1)} \mathbf{v}_2 + a_r^{(2)} \mathbf{v}_4 \tag{5b}$$

and

$$\begin{bmatrix} \mathbf{E}_t \\ \mathbf{H}_t \end{bmatrix} = a_t^{(1)} \mathbf{v}_1 + a_t^{(2)} \mathbf{v}_3 \tag{5c}$$

in which $a_i^{(1)}$, $a_i^{(2)}$, are the mode coefficients of the incident field and $a_r^{(1)}$, $a_r^{(2)}$, $a_t^{(1)}$, $a_t^{(2)}$ are the unknown coefficients for the reflected and transmitted modes. We proceed to determine these coefficients by introducing the unit cell transfer matrix $\bar{\mathbf{T}}$, such that

$$\left[a_r^{(1)} a_r^{(2)} a_t^{(1)} a_t^{(2)}\right]^T = [(-\bar{\mathbf{T}}^N \mathbf{v}_2)(-\bar{\mathbf{T}}^N \mathbf{v}_4)\mathbf{v}_1 \mathbf{v}_3]^{-1} \times \left[a_i^{(1)} \bar{\mathbf{T}}^N \mathbf{v}_1 + a_i^{(2)} \bar{\mathbf{T}}^N \mathbf{v}_3\right] \tag{6}$$

in which N refers to the total number of unit cells. To obtain the intermediate field distribution along the crystal, we can successively multiply the field at the beginning of the structure with the unit cell transfer matrix $\bar{\mathbf{T}}$.

Although the above procedure is simple, numerical instabilities appear when the MPC slab consists of many periodic layers. This is especially true when the excitation is close to the bandgap frequencies. We can overcome this difficulty by dividing the crystal into smaller multicell stacks and by subsequently applying the transfer matrix analysis to each of these stacks separately. Recombination of all equations into a single matrix system results in a numerically stable and efficient scheme for large N. As an example, let us consider the three section region shown in Fig. 5. For this specific case, we express the intermediate field values in terms of the plane wave modes within the F layer (assuming all subdivisions end with the last layer, and begin with the first layer of the unit cell). The F layer modes can be represented as a combination of the plane wave modes $\mathbf{e}_{f1} e^{iq_{f1} z}, \mathbf{e}_{f2} e^{-iq_{f1} z}, \mathbf{e}_{f3} e^{iq_{f2} z}$, and $\mathbf{e}_{f4} e^{-iq_{f2} z}$ (q_{f1} and q_{f2} being the supported wavenumbers). The unknown coefficients a_k^j and b_k^j for the jth mode in the kth interval can then be related to $\mathbf{e}_{f1}, \mathbf{e}_{f2}, \mathbf{e}_{f3}$, and $\mathbf{e}_{f4}$ by solving the system

$$\bar{\mathbf{T}}_1 \left[a_i^{(1)} \mathbf{v}_1 + a_i^{(2)} \mathbf{v}_3 + a_r^{(1)} \mathbf{v}_2 + a_r^{(2)} \mathbf{v}_4\right] = \left[a_1^{(1)} \mathbf{e}_{f1} + a_1^{(2)} \mathbf{e}_{f3} + b_1^{(1)} \mathbf{e}_{f2} + b_1^{(2)} \mathbf{e}_{f4}\right] \tag{7a}$$

$$\bar{\mathbf{T}}_2\left[a_1^{(1)}\mathbf{e}_{f1}+a_1^{(2)}\mathbf{e}_{f3}+b_1^{(1)}\mathbf{e}_{f2}+b_1^{(2)}\mathbf{e}_{f4}\right] = \left[a_2^{(1)}\mathbf{e}_{f1}+a_2^{(2)}\mathbf{e}_{f3}+b_2^{(1)}\mathbf{e}_{f2}+b_2^{(2)}\mathbf{e}_{f4}\right] \quad (7b)$$

$$\bar{\mathbf{T}}_3\left[a_2^{(1)}\mathbf{e}_{f1}+a_2^{(2)}\mathbf{e}_{f3}+b_2^{(1)}\mathbf{e}_{f2}+b_2^{(2)}\mathbf{e}_{f4}\right] = \left[a_t^{(1)}\mathbf{v}_1+a_t^{(2)}\mathbf{v}_3\right] \quad (7c)$$

for the positive and negative propagating modes respectively, where $\mathbf{v}_j$'s are again used to represent the free space plane wave modes. We remark that the coefficients $a_i^{(1)}, a_i^{(2)}, a_r^{(1)}, a_r^{(2)}, a_t^{(1)}$, and $a_t^{(2)}$ are the same as those defined in (6). Knowledge of all unknown coefficients also yields the fields at the interfaces of the multicell stacks. Within each stack, the fields can be found by successive $\bar{\mathbf{T}}$ multiplications with the field values at the incidence boundary of the stack. Thus, errors due to successive multiplications are confined within each individual multicell stack and instabilities are avoided. Once the field distributions for multiple frequencies have been determined, fields in time domain can be generated via Fourier transform. Using this method, we next proceed to investigate the propagation characteristics of a narrow band RF Gaussian pulse inside the magnetic crystal. As noted above, of particular interest is the case when the pulse is modulated around the frozen mode frequency ω_s.

III. Propagation in Lossless Magnetic Photonic Crystals

In [16], Bloch wave analysis was used to demonstrate the strong bulk asymmetry in the frequency spectrum of ideal lossless MPCs, having sufficient Faraday rotation in the F layers and appropriate misalignment of the A layers. Further, in [17] the existence of a *stationary* inflection point associated with the conditions $\omega'(k)=\omega''(k)=0, \omega'''(k)\neq 0$ was shown. At this stationary inflection point, the Bloch modes of the MPC degenerate into general divergent Floquet modes. Concurrently they are associated with vanishing group velocity and therefore referred to as frozen modes. Nevertheless, [16] and [17] assumed semi-infinite crystal media, but for practical applications it is of interest to consider finite thickness crystal slabs. In this section, we examine propagation within the frozen mode regime (frequency band near the occurrence of the frozen mode frequency) for the case of a finite slab. Specifically, we will present results to demonstrate the coupling, amplitude growth, propagation speed, and field distribution of these frozen modes for a lossless MPC slab.

The A layer constitutive tensors in (3a) and (3b) represent anisotropic dielectric materials which are aligned with an angle ϕ_A about their primary z axis. Among the naturally available anisotropic crystals, we will consider "rutile" (a uniaxial crystal) for the A layers. Rutile (TiO_2) has a dielectric constant of $\epsilon_a = 125$ and $\delta = 40$ [see (3a)] with corresponding loss tangents of $\tan\delta_{\epsilon_a} = 9.32\times 10^{-5}$ and $\tan\delta_{\delta} = 1.2125\times 10^{-4}$, respectively. On the other hand, the F layer tensors in (4a) and (4b) describe gyromagnetic materials having a primary axis along z. The imaginary off-diagonal entries describe the well known Faraday rotation effect with the ratio β/μ. This ratio and the total length of the layer determines the amount of Faraday rotation the wave would acquire upon crossing the layer. Properly magnetized soft ferrites, such as yttrium iron garnet (YIG), can be used to construct the F layers.

The permeability tensors of ferrites can be well approximated by the Lorentz curves as (see [19])

$$\bar{\bar{\mu}}_F = \mu_0\begin{bmatrix}\mu & i\beta & 0\\ -i\beta & \mu & 0\\ 0 & 0 & \mu_{fz}\end{bmatrix} = \mu_0\begin{bmatrix}1&0&0\\0&1&0\\0&0&1\end{bmatrix} + \mu_0\frac{\gamma M_0}{(\omega_0^2-\omega^2)}\begin{bmatrix}\omega_0 & i\omega & 0\\ -i\omega & \omega_0 & 0\\ 0&0&0\end{bmatrix} \quad (8a)$$

where

$$\omega_0 = \omega_H - i\alpha\omega,\ \ \omega_H = \gamma H_0,\ \ \alpha = \frac{\gamma\Delta H}{2\omega},\ \ \gamma \approx 1.4g\frac{\text{MHz}}{\text{Oe}}$$

with ω_H being the magnetic resonance frequency, γ is the gyromagnetic ratio obtained from the experimental factor g, ΔH is the linewidth of the Lorentz curve, and α is the parameter associated with dissipation within the crystal. Also, M_0 is the usual saturation magnetization parameter of the ferrite and H_0 is the static magnetic bias field. It is important to note that H_0 must be large enough to put the ferrite into saturation. For the F layers, we will consider a narrow linewidth ferrite. More specifically, calcium vanadium garnet (CVG) with $\Delta H = 1$ Oe, $g = 2.01$, $M_0 = 1950$ G will be assumed to form the F layers. Also, for our analysis a narrowband pulse will be considered. Since we operate away from the ferromagnetic resonance region (to keep losses at a minimum) and the pulse is narrow band, the permeability tensor can be assumed constant over the analysis band. This allows for a constant loss tangent as well. Specifically, at 10 GHz, with $H_0 = 5.95$ kOe, we note that the F layer permeability parameters to be used are $\mu = 1.6701, \beta = 0.4497$ with the loss tangents given by $\tan\delta_\mu = 0.0001, \tan\delta_\beta = 0.000\,34$. Also, the dielectric constant of CVG is $\epsilon_f = 14.5$ with $\tan\delta = 0.0001$.

To consider wave propagation within the MPC, we start our analysis by first assuming no losses within the crystal (losses will be considered in the subsequent section). Specifically, we set the A layer (rutile) material parameters to $\epsilon_a = 125, \delta = 40$ with $\phi_{A1} = 0$, and $\phi_{A2} = -\pi/12$. For the CVG F layers the material parameters are set as above ($\epsilon_f = 14.5, \mu = 1.6701$, and $\beta = 0.4497$). Furthermore, the thickness of the F layer is scaled relative to that of the A layer. That is, a thickness of $F = 0.5$ implies that the F layer is half as thick as the A layer. For our examples, the A layer thicknesses were set to 0.5695 mm. Before proceeding further, we should stress that although the individual layers of the MPC are assumed to be nondispersive, the assembled MPC exhibits strong dispersive characteristics as will be discussed next.

Fig. 6 provides a closer view of the band diagram for various F layer thicknesses near the frozen mode frequency. Of particular interest is the bending of the curves at the inflection region as the thickness of the F layer is varied. For the case of $F = 0.39$, although the curve does indeed have an inflection point ($\omega''(k) = 0$), we note that it is not stationary. However, by adjusting the aspect ratio of the layers, the slope of the curve can be made to approach zero, $\omega'(k) \to 0$. Specifically, the case of

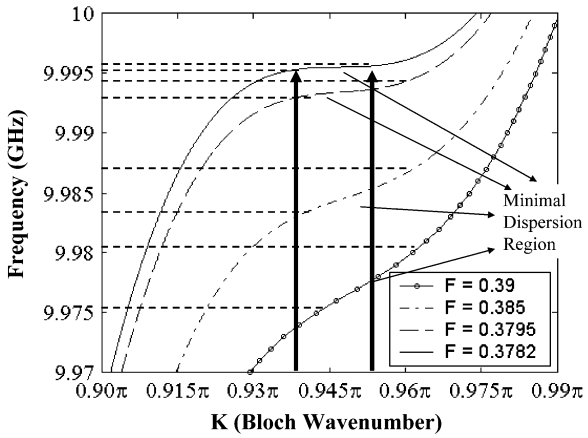

Fig. 6. Band diagram for different ferrite layer thicknesses.

$F = 0.3782$ leads to a curve that nearly exhibits the stationary inflection point at $k = 0.945\pi$. As seen, a slight variation in the thickness of the F layer leads to lower slopes at the inflection region. Of course, the slope is associated with the wave velocity and the location where this velocity vanishes defines the stationary inflection point that the frozen mode frequency occurs. It is important that we operate within the minimal dispersion region (almost linear segment) of the k-ω curve near the frozen mode point to avoid dispersion. Hence, to a great degree, the extent of the linear segment around the frozen mode frequency (to be referred to as the frozen mode regime) defines the bandwidth of the crystal if we chose to retain the same biasing magnetic field. As an example, for $F = 0.3782$ the linear segment occurs approximately within the region $0.935\pi < K < 0.958\pi$ of the k-ω curve. Outside this frozen mode regime propagation within the crystal is highly dispersive.

Let us now consider the propagation of a Gaussian pulse in a slab consisting of a periodic arrangement of the crystal layers $(N = 2000)$ corresponding to $F = 0.3795$ (dashed curve in Fig. 6). Fig. 7(a) is a time snapshot of the incident electric field that is linearly polarized in x. We note, however, that due to the anisotropic nature of the A layers and gyromagnetic nature of the F layers, the wave inside the MPC has a general elliptical polarization. The x-component of the electric field inside the MPC is shown in Fig. 7(b) at $38.938\ \mu$s. Throughout the paper, the time origin $(t = 0)$ corresponds to the instant when the incident pulse peak is D meters away from the MPC boundary (for the above case $D = 7500$ m). Of particular importance is that the pulse shape is retained (very low dispersion) implying that the information content potentially carried by the pulse is also retained. As expected, the pulse shrinks significantly and is enlarged in amplitude (due to the intrinsic multiple reflections within the crystal). More specifically, the amplitude of the interior field increases by a factor of 5.7 for this case and the pulse width shrinks by a factor of nearly 3000 (original spatial width of $250\,000\lambda_0$ is reduced to $80\lambda_0$). Table I summarizes the corresponding D values as well as the spatial variances of the incident Gaussian pulses (σ) for different F layer thicknesses. The envelope of the Gaussian pulse is thus expressed as $e^{-(z+D)^2/2\sigma^2}$. We note here that, since the minimum dispersion bandwidth (BW) of the MPC varies with the F layer thickness, the spatial extent of the incident pulse, σ, must also be adjusted

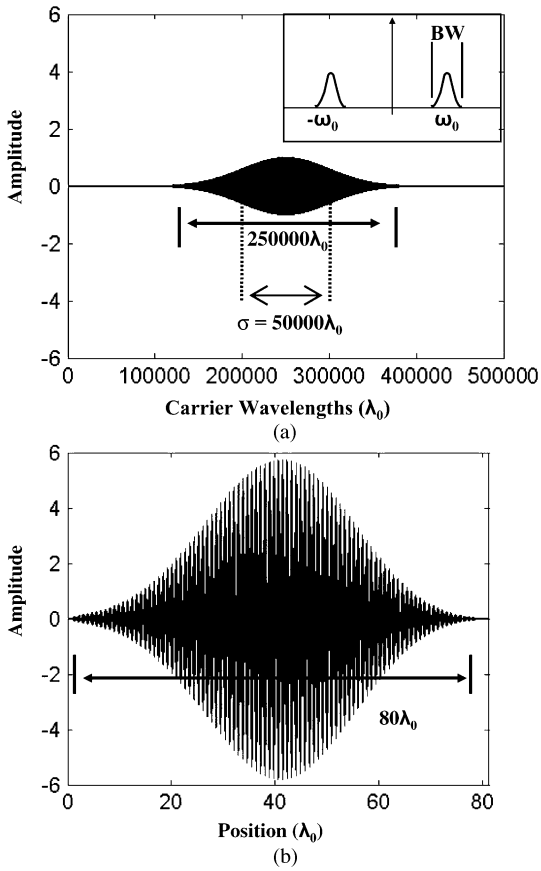

Fig. 7. (a) Input pulse in free space and (b) E_x distribution in crystal when $t = 38.938\ \mu$s, $F = 0.3795$, $D = 7500$m, $N = 2000$ (see Table I).

TABLE I
PROPAGATION CHARACTERISTICS OF MAGNETIC PHOTONIC CRYSTALS

F	D / σ (10^3m)	Freq.±BW (GHz)	Min. thickness	Max. amp.	Pulse speed
0.39	0.21 / 0.045	9.977531± 0.00350	$2.25\lambda_0$	1.9	$c/420$
0.385	0.9 / 0.105	9.985065± 0.00150	$2.27\lambda_0$	2.52	$c/700$
0.3795	7.5 / 1.5	9.993420± 0.00010	$4\lambda_0$	5.7	$c/3660$
0.3782	48 / 11.4	9.995523± 0.000012	$10.65\lambda_0$	14.3	$c/25000$

accordingly. This leads to different D values to ensure that at $t = 0$, D is far enough so that most of the incident pulse is outside of the MPC.

Fig. 8(a)–(c) gives a more expanded and detailed history of the incident pulse coupling and propagating inside the MPC by considering the initial part $(0\lambda_0 - 4\lambda_0)$ of the MPC in Fig. 7(b). Specifically, Fig. 8(a) shows the pulse at $13.936\ \mu$s whereas Fig. 8(b) and (c) gives the pulse shape at $19.059\ \mu$s and $25.51\ \mu$s, respectively. Here, we are particularly interested in observing how quickly the pulse reaches its maximum field strength once inside the crystal. In this example, the pulse reaches its maximum amplitude within $4\lambda_0$ (≈ 12 cm). As shown in Fig. 9, by adjusting the thickness of the ferrite layer to be $F = 0.3782$ (implying a flatter slope around the inflection point) the pulse can reach a maximum amplitude of 14 within $11\lambda_0$ (higher amplitude and longer propagation). That is, as the frequency of oper-

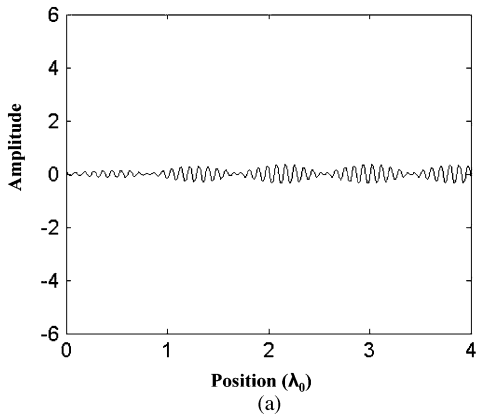

(a)

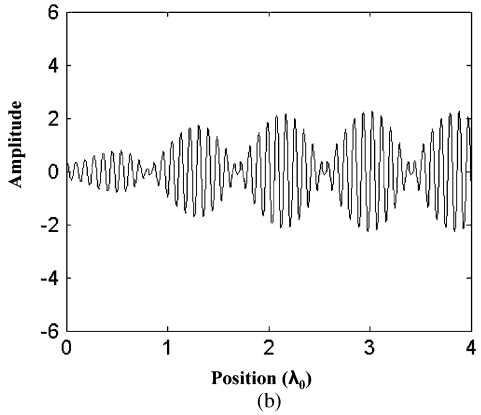

(b)

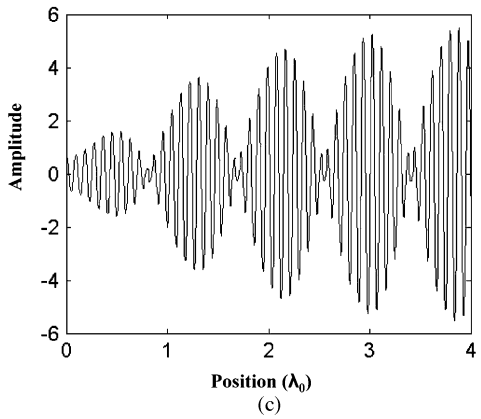

(c)

Fig. 8. (a)–(c) Snapshots of the E_x field at $t = 13.936\ \mu$s, $t = 19.059\ \mu$s, and $t = 25.51\ \mu$s in case $F = 0.3795$, $D = 7500$ m, $N = 2000$ (see Table I).

ation and the slope of the k-ω curve gets closer to the stationary inflection point, the amplitude grows remarkably.

Achieving a maximum amplitude within a small distance once inside the crystal is critically important since it translates to smaller slab thicknesses, an important factor for practical realizations. Table I summarizes the characteristics of the propagating pulse for different ferrite layer thicknesses when the incident electric field is an x-polarized Gaussian pulse of unity magnitude. To generate the table, we chose $N = 600$ (number of unit cells) for the cases of $F = 0.39$ and $F = 0.385$. However, the number of unit cells was increased to $N = 2000$ for $F = 0.3795$ and to $N = 2500$ for $F = 0.3782$. This ensured that the entire transmitted pulse would fit within the crystal width (the bandwidth in Table I is changing for different F layers to accommodate the minimal dispersion region). As already noted, the maximum amplitude increases significantly

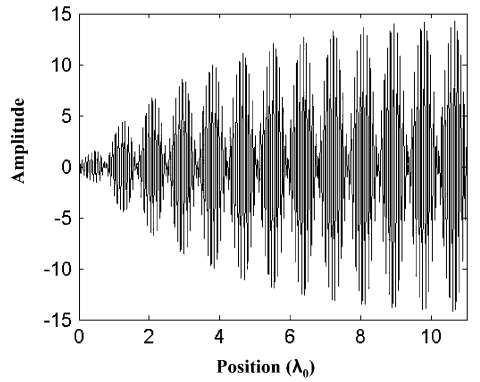

Fig. 9. E_x at $t = 172.52\ \mu$s in case $F = 0.3782, D = 48\,000$ m, $N = 2500$ (see Table I).

when the thickness of the F layer is adjusted for a flatter k-ω curve. However, we note here that decreasing the F layer thickness further will cause the k-ω curve to bend inward, causing the frozen mode regime to disappear. Concurrently, the allowable bandwidth for dispersion–free propagation decreases (the minimal dispersion region narrows as shown in Fig. 6). The slab thickness needed to achieve the maximum pulse amplitude also increases as the k-ω curve is made flatter.

The remarkable and unique property of the proposed MPC can also be seen from the last two columns in Table I, where the interior pulse amplitude increases by a factor of 14 and the speed is reduced to $(1/25\,000)$th of the original propagation velocity. Even for the case when $F = 0.39$, the propagation speed of the pulse decreases to $(1/420)$th of that in free space. Such slow-down in speed is expected to allow for RF device miniaturization when such crystals can be used as the host medium. Correspondingly, to achieve such a slow speed using uniform and homogenous media, the relative permittivity ϵ_r must be as high as 176 400. Even if such a high dielectric constant structure is available, reflections and mismatches at the air-dielectric interfaces would prevent EM coupling into the material. On the contrary, the most unique aspect of the MPC is that it concurrently exhibits negligible backward reflection when operating in the minimal dispersion region near the frozen mode frequency [17]. The transmittance of the MPC calculated from the Bloch analysis for the semi-infinite case is shown in Fig. 10 for different F layer thicknesses and for an x-polarized incident field. As seen, the highest transmittance occurs at the frozen mode frequency and it is more than 70% (up to 85%) for all cases. Moreover, the transmittance improves as the k-ω curve is made flatter near the frozen mode frequency as the F layer thickness is varied.

Slow-down and amplitude growth within the MPC are consequences of multiple reflections that occur at the frozen mode regime. The snapshots of the instantaneous power density $\hat{\mathbf{z}} \cdot (\bar{\mathbf{E}} \times \bar{\mathbf{H}})$ shown in Fig. 11(a) for the $F = 0.3795$ case clearly depicts the effect of reflections. We observe that the power density has large positive and negative values ($-z$ directed instantaneous power density) with respect to the peak of the incident instantaneous power $(+1)$. The pulse is basically squeezed within the MPC and its time harmonic components reflect back and forth causing a small net positive group velocity with large field amplitudes. The average power calculated by integrating the instantaneous power over a finite spatial

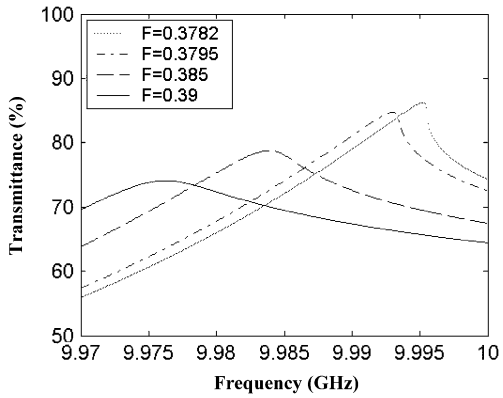

Fig. 10. Transmittance of the MPC for different F thicknesses.

window is a smooth Gaussian curve as shown in Fig. 11(b). As expected, the maximum of the average power matches the transmitted power ($\approx 80\%$ of the average incident power for this example). Further, we remark that once the spatial extent of the transmitted pulse is scaled by the pulse propagation speed ($c/3660$ in this case), we simply recover the incident power curve in Fig. 11(c).

IV. Material Loss Effects on Propagation

In the previous section, we considered an ideal lossless MPC structure. We demonstrated that the Bloch spectrum is nonreciprocal and can have a stationary inflection point (frozen mode frequency). We also presented the propagation characteristics of the MPC medium when excited at or near the frozen mode frequency. Nevertheless, the above study did not account for losses usually found in realistic materials. Therefore, it is equally important to examine the effects of material loss on the frozen mode phenomenon. Thus, in this section we focus on the same MPC structure but with losses incorporated within the crystals.

Table II presents the propagation properties for a realistic MPC having a loss tangent of the order $\tan\delta \approx 10^{-4}$ (as given in Section III) and for an ultra low loss MPC with $\tan\delta \approx 10^{-5}$. As before, the MPC is illuminated with the same incident field used to generate Table I. As seen from Table II, a significant increase in amplitude at the frozen mode regime is again observed. However, the amplitude is reduced by more than 50% even for the case of $\tan\delta = 10^{-5}$. This higher loss is likely due to the multiple reflections within the crystals, viz. the same behavior that results in pulse compression. Nevertheless, it is important to note the amount of total loss is also strongly dependent on the slope of the k-ω curve. This implies that a trade-off between loss and the maximum (peak) amplitude can be achieved within the crystal. In this vein, we remark that decreasing the loss tangent from 10^{-4} down to 10^{-5} results in nearly doubling the peak amplitude from 2.6 up to 5.7. Accordingly, it is crucial to choose low loss materials for the design of MPC and to concurrently adjust the stationary inflection point to achieve maximum amplitude for the given loss tangent of the material.

To further illustrate the loss in the MPC and its dependence on the slope at the inflection region, we proceed by considering a time harmonic field excitation. We specifically concentrate on

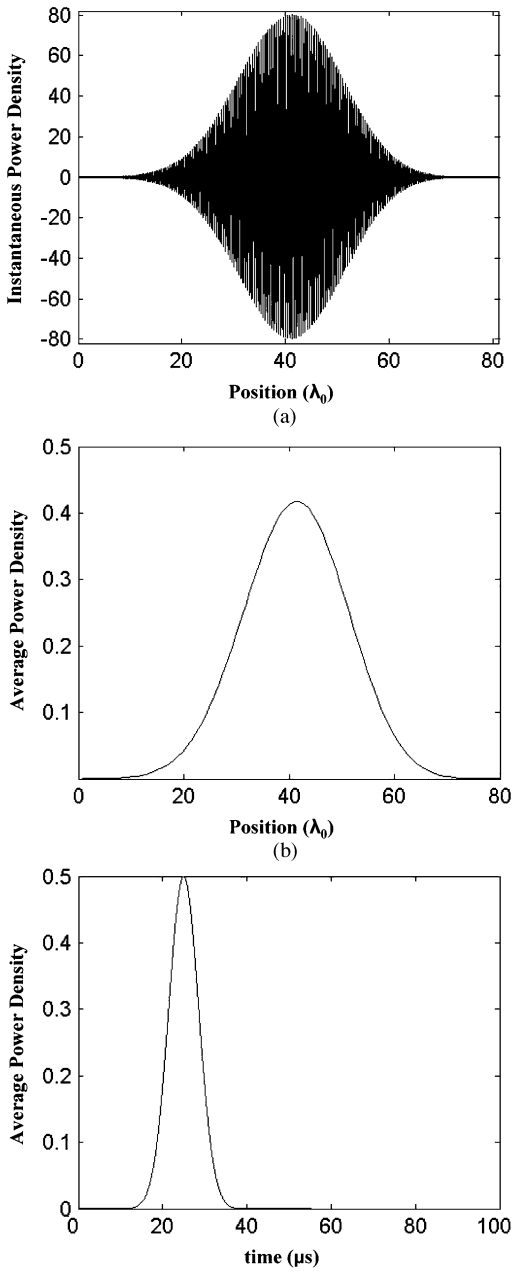

Fig. 11. (a) Instantaneous power density $\hat{\mathbf{z}}\cdot(\bar{\mathbf{E}}\times\bar{\mathbf{H}})$ snapshot in the MPC. (b) Average power in the MPC for $F = 0.3795$. (c) Average power of the incident field in time domain observed at the leftmost boundary of the MPC.

the envelope of the electric field within the MPC for two different loss tangents. For this case, we choose a large number of unit cells ($N = 2000$) to emulate a semi-infinite medium. Fig. 12(a)–(d) present the envelope of the electric field as a function of position within the MPC for various F layer thicknesses. We clearly observe that the envelopes attenuate faster as the k-ω curve is made flatter by adjusting the F layer thickness. This is likely due to the higher pulse compression implying that more bounces occur within the crystal prior to reaching a steady-state condition. We note that a nonmonotonic decay as shown in Fig. 12(c) and (d) is associated with the field component. When the power density is actually plotted the corresponding curve is monotonic.

TABLE II
EFFECT OF LOSS ON PROPAGATION CHARACTERISTICS

F	D (10^3m)	σ (10^3m)	Freq.±BW (GHz)	Min. thickness	Max. amp.	Min. thickness	Max. amp.	Pulse speed
0.39	0.21	0.045	9.977531 ± 0.00350	$1.62\lambda_0$	1.62	$2\lambda_0$	1.85	$c/420$
0.385	0.9	0.105	9.985065 ± 0.00150	$1.3\lambda_0$	1.95	$2.2\lambda_0$	2.4	$c/700$
0.3795	7.5	1.5	9.993420 ± 0.00010	$1.3\lambda_0$	2.5	$3.1\lambda_0$	4.36	$c/3660$
0.3782	48	11.4	9.995523 ± 0.000012	$1.2\lambda_0$	2.6	$3\lambda_0$	5.7	$c/25000$
				$\tan\delta \approx 10^{-4}$		$\tan\delta \approx 10^{-5}$		

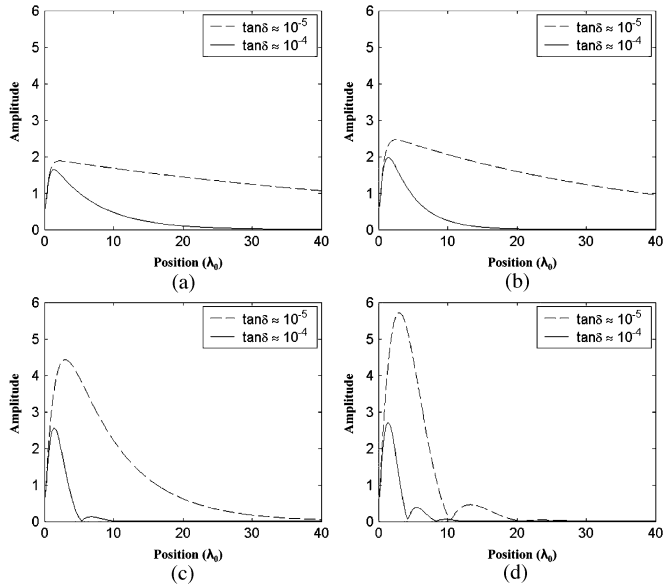

Fig. 12. Envelope of E_x in the MPC at the carrier frequency (a) $F = 0.39$, (b) $F = 0.385$, (c) $F = 0.3795$, and (d) $F = 0.3782$.

V. CONCLUDING REMARKS

We presented a study of the electromagnetic wave propagation characteristics within a class of MPCs constructed from a periodic arrangement of available homogeneous material layers. These crystals are unidirectional and have the unique property of exhibiting concurrent low reflectivity and dramatic wave slow-down coupled with a large wave amplitude increase once within the MPC. That is, they exhibit very large effective dielectric constant, but can still display low reflectance for an externally impinging pulse. These concurrent phenomena occur at and near a specific frequency referred to as the frozen mode, and can be potentially exploited for improved antenna matching and miniaturization.

Our study focused on practical/realizable finite dielectric slab configurations and on the existence and characteristics of the aforementioned phenomena when the crystals are comprised of available materials. We observed that once inside the MPC, the spatial width of an incident harmonic Gaussian pulse decreases whereas its field amplitude increases remarkably. Specifically, very slow group velocities on the order of $c/25\,000$, where c is the speed of light, are possible within the MPC with a concurrent transmittance of greater than 70%. However, to retain large wave amplitudes with minimal dispersion, one must operate within a small bandwidth around the frozen mode frequency. The spatial location where the pulse reaches its maximum amplitude is also strongly dependent on the slope of the k-ω curve. Of course, the periodic slab forming the MPC must have a minimum thickness to realize the possible maximum wave amplitude. We should remark that magnetic biasing can be used to increase the realizable bandwidth based on the properties of the ferrite layer used to form the crystal.

We considered, both ideal (lossless) as well as material layers exhibiting practical losses. The interesting MPC phenomena are indeed present and realized when the crystals have finite loss tangents. However, the wave amplitude increase is reduced in a manner controlled by the slope of the k-ω diagram at the frozen mode frequency. Thus, given the specific materials comprising the MPC, a compromise between amplitude growth and bandwidth (without biasing) is needed to achieve the best utilization of the crystal for a specific application. Specifically, for the low loss materials $(\tan\delta = 10^{-4})$ discussed throughout the paper, the amplitude of E_x can be increased by 20% but concurrently the bandwidth is reduced by as much as 70% (see Table II). That is, a small amplitude increase can imply a large bandwidth compromise. Of course, there are many parameters that play a role in the amplitude versus bandwidth choices. Among them are the anisotropy ratios and dielectric constants, loss tangents, misalignment angles among layers, biasing and ferrite layer characteristics. The practical compromise among these choices is under investigation.

REFERENCES

[1] D. Polder, "On the theory of ferromagnetic resonance," *Phil. Mag.*, vol. 40, pp. 99–115, Jan. 1949.
[2] G. Tyras, "The permeability matrix for a ferrite medium magnetized at an arbitrary direction and its eigenvalues," *IRE Trans. Microwave Theory Tech.*, vol. MTT-7, no. 1, pp. 176–177, Jan. 1959.
[3] H. Gundel, H. Riege, E. Wilson, J. Handerek, and K. Zioutas, "Fast polarization changes in ferroelectrics and their application in accelerators," *Nucl. Instrum. Methods Phys. Res. A*, vol. 280, pp. 1–6, 1989.
[4] X. Zuo, H. How, S. A. Oliver, and C. Vittoria, "Development of high frequency ferrite phase-shifter," *IEEE Trans. Magn.*, vol. 37, no. 4, pp. 2395–2397, Jul. 2001.
[5] H. How, P. Shi, C. Vittoria, E. Hokanson, M. H. Champion, L. C. Kempel, and K. D. Trott, "Steerable phased array antennas using single-crystal YIG phase shifters—Theory and experiments," *IEEE Trans. Microw. Theory Tech.*, vol. 48, no. 9, pp. 1544–1549, Sep. 2000.
[6] A. D. Brown, J. L. Volakis, L. C. Kempel, and Y. Y. Botros, "Patch antennas on ferromagnetic substrates," *IEEE Trans. Antennas Propag.*, vol. 47, no. 1, pp. 26–32, Jan. 1999.
[7] A. C. Polycarpou, C. A. Balanis, J. T. Aberle, and C. Britcher, "Radiation and scattering from ferrite tuned cavity backed slot antennas: Theory and experiment," *IEEE Trans. Antennas Propag.*, vol. 46, no. 9, pp. 1297–1306, Sep. 1998.
[8] E. Yablonovich, "Inhibited spontaneous emission in solid-state physics and electronics," *Phys. Rev. Lett.*, vol. 58, p. 2059, 1987.

[9] A. Grbic and G. V. Eleftheriades, "Overcoming the diffraction limit with a planar left handed transmission line lens," *Phys. Rev. Lett.*, vol. 92, no. 11, pp. 117 403 1–117 403 4, Mar. 2004.
[10] F. Yang and Y. Rahmat-Samii, "A low profile circularly polarized curl antenna over an electromagnetic bandgap (EBG) surface," *Microw. Opt. Tech. Lett.*, vol. 31, no. 4, pp. 264–267, Nov. 2001.
[11] R. F. J. Broas, D. F. Sievenpiper, and E. Yablonovitch, "A high-impedance ground plane applied to a cellphone handset geometry," *IEEE Trans. Microw. Theory Tech.*, vol. 49, no. 7, pp. 1262–1265, Jul. 2001.
[12] Y. E. Erdemli, K. Sertel, R. A. Gilbert, D. E. Wright, and J. L. Volakis, "Frequency-selective surfaces to enhance performance of broad-band reconfigurable arrays," *IEEE Trans. Antennas Propag.*, vol. 50, no. 12, pp. 1716–1724, Dec. 2002.
[13] G. Kiziltas, D. Psychoudakis, J. L. Volakis, and N. Kikuchi, "Topology design optimization of dielectric substrates for bandwidth improvement of a patch antenna," *IEEE Trans. Antennas Propag.*, vol. 51, no. 10, pp. 2732–2743, Oct. 2003.
[14] M. A. Antoniades and G. V. Eleftheriades, "Compact linear lead/lag metamaterial phase shifters for broadband applications," *IEEE Antennas Wireless Propag. Lett.*, vol. 2, no. 7, pp. 103–106, Jul. 2003.
[15] J. Joannopoulos, R. Meade, and J. Winn, *Photonic Crystals - Molding the Flow of Light.*. Princeton, NJ: Princeton Univ. Press, 1995.
[16] A. Figotin and I. Vitebsky, "Nonreciprocal magnetic photonic crystals," *Phys. Review. E*, vol. 63, pp. 066 609 1–066 609 20, May 2001.
[17] A. Figotin and I. Vitebskiy, "Electromagnetic unidirectionality in magnetic photonic crystals," *Phy. Rev. B*, vol. 67, pp. 165 210 1–165 210 20, Apr. 2003.
[18] R. E. Collin, *Field Theory of Guided Waves.*. New York, NY: IEEE Press, 1991.
[19] A. G. Gurevich and G. A. Melkov, *Magnetization Oscillations and Waves.*. Boca Raton, FL: CRC Press, 1996.

Gokhan Mumcu (S'03) was born on March 30, 1982 in Bursa, Turkey. He received the B.S. degree from Bilkent University, Ankara, Turkey and the M.S. degree from The Ohio State University, Columbus, all in electrical engineering, in 2003 and 2005, respectively.

He is currently working toward the Ph.D. degree in the ElectroScience Laboratory, The Ohio State University, as a Graduate Research Associate. His research areas include electromagnetic theory, computational electromagnetics, and metamaterials.

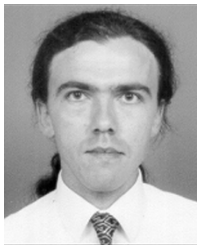

Kubilay Sertel (M'03) was born on June 27, 1973, in Tekirdag, Turkey. He received the B.S. degree from Middle East Technical University, Ankara, Turkey, in 1995, the M.S. degree from Bilkent University, Ankara, Turkey, in 1997, and the Ph.D. degree from the Electrical Engineering and Computer Science Department, University of Michigan, Ann Arbor, in 2003.

He is currently a Senior Research Associate at the ElectroScience Laboratory, The Ohio State University, Columbus. His research areas include electromagnetic theory, computational electromagnetics, integral equation and hybrid methods, fast and efficient methods for large-scale electromagnetics problems and parallel implementations of fast algorithms.

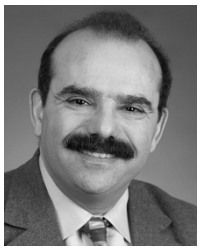

John L. Volakis (S'77–M'82–SM'89–F'96) was born on May 13, 1956, in Chios, Greece. He received the B.E. degree (*summa cum laude*) from Youngstown State University, Youngstown, OH, in 1978 and the M.Sc. and Ph.D. degrees The Ohio State University, Columbus, in 1979 and 1982, respectively.

From 1982 to 1984, he was with Rockwell International, Aircraft Division, Lakewood, CA, and during 1978 to 1982, he was a Graduate Research Associate at the ElectroScience Laboratory, The Ohio State University. From 1984 to 2002, he was a Professor in the Electrical Engineering and Computer Science Department, University of Michigan, Ann Arbor, where from 1998 to 2000, he also served as the Director of the Radiation Laboratory. Since January 2003, he has been the Roy and Lois Chope Chair Professor of Engineering at The Ohio State University, Columbus, and also serves as the Director of the ElectroScience Laboratory. He has published over 220 articles in major refereed journal articles (nine of these have appeared in reprint volumes), more than 250 conference papers and ten book chapters. In addition, he coauthored two books *Approximate Boundary Conditions in Electromagnetics* (London, U.K.: IEE, 1995) and *Finite Element Method for Electromagnetics* (New York: IEEE Press, 1998). From 1994 to 1997, he was an Associate Editor of *Radio Science* and is currently an Associate Editor for the *Journal of Electromagnetic Waves and Applications*. He has also written two well-edited coursepacks on introductory and advanced numerical methods for electromagnetics, and has delivered short courses on numerical methods, antennas and frequency selective surfaces. His primary research deals with computational methods, electromagnetic compatibility and interference, design of new RF materials, multiphysics engineering and bioelectromagnetics.

Dr. Volakis is a Member of Sigma Xi, Tau Beta Pi, Phi Kappa Phi, and Commissions B and E of the International Union of Radio Science (URSI). In 1998, he received the University of Michigan College of Engineering Research Excellence award and in 2001 he received the Department of Electrical Engineering and Computer Science Service Excellence Award. He graduated/mentored 40 Ph.D. students/postdoctorates, and coauthored with them five papers receiving best paper awards at conferences. He served as an Associate Editor of the IEEE TRANSACTIONS ON ANTENNAS AND PROPAGATION from 1988 to 1992, and is currently an Associate Editor for the IEEE ANTENNAS AND PROPAGATION SOCIETY MAGAZINE and the *URSI Bulletin*. He chaired the 1993 IEEE Antennas and Propagation Society Symposium and Radio Science Meeting, and was a Member of the AdCom for the IEEE Antennas and Propagation Society from 1995 to 1998. He served as the 2004 President of the IEEE Antennas and Propagation Society. He is listed by ISI among the top 250 most referenced authors (2004, 2005).

Ilya Vitebskiy was born on November 5, 1950 in Murmansk, Russia, and immigrated to the U.S.A. in 1994. He received the M.Sc. and the Ph.D. degrees, both in physics, and the degree of Doctor of Physical and Mathematical Sciences, from Donetsk State University, Donetsk, U.S.S.R., (now the Ukraine) in 1972, 1979, and 1985, respectively.

From 1974 though 1987, he was a Research Fellow in the Institute of Physics and Technology of Ukrainian Academy of Science, Donetsk State University. From 1988 until 1995, he headed the Department of Rheoretical Physics in the Institute for Single Crystals, Kharkov (Former U.S.S.R.), where he also worked as a professor of theoretical physics. Since 1986, he graduated six Ph.D. students, all in the area of solid state physics. After he moved to the United States in 1995, he worked for small research and development companies SageTech, Inc., Marietta, GA and PDH International, Decatur, GA, as a Chief Scientist and Vice President of Technology. During this time he was involved in different projects related to the electrodynamics of photonic crystals, and received by the Air Force Office of Scientific Research. Since 2000, he has been a Researcher at the University of California at Irvine, working on the projects in the area of electrodynamics of composite media. As a co-inventor, he was awarded four U.S. patents and has and two patents pending. He is an author and coauthor of 96 scientific papers in peer-reviewed journals. His area of expertise covers various aspects of solid state theory, including theory of electromagnetic and acoustic properties of crystalline materials, magnetic resonance and spin waves, phase transitions and critical phenomena, electrodynamics of composite media.

Alexander Figotin was born in Kharkov, U.S.S.R., in 1954. He received the Ph.D. in mathematics from Tashkent State University, Tashkent, U.S.S.R., in 1980.

Currently he is a Professor at the University of California at Irvine. He published more than 60 papers and one monograph. His area of expertise includes wave propagation in periodic and random media, theory of linear and nonlinear photonic crystals, spectral theory of dispersive and dissipative dielectric and other media, random number generation.